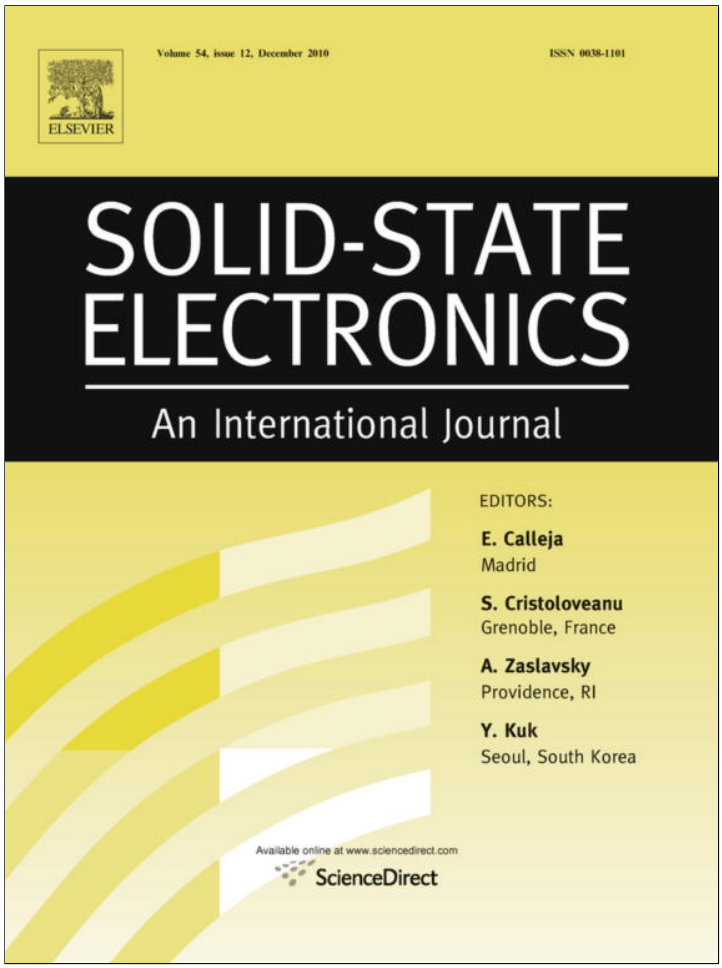

Solid-State Electronics 54 (2010) 1586–1591

Contents lists available at ScienceDirect

Solid-State Electronics

journal homepage: www.elsevier.com/locate/sse

Analytical modeling of quantum threshold voltage for triple gate MOSFET

P. Rakesh Kumar *, Santanu Mahapatra

Nano Scale Device Research Laboratory, Centre for Electronics Design and Technology, Indian Institute of Science, Bangalore 560012, India

ARTICLE INFO

Article history:
Received 10 February 2010
Received in revised form 16 July 2010
Accepted 22 July 2010
Available online 21 August 2010

The review of this paper was arranged by S. Cristoloveanu

Keywords:
Compact modeling
Quantum threshold voltage
MOSFET
Device simulation

ABSTRACT

In this work, a physically based analytical quantum threshold voltage model for the triple gate long channel metal oxide semiconductor field effect transistor is developed. The proposed model is based on the analytical solution of two-dimensional Poisson and two-dimensional Schrödinger equation. Proposed model is extended for short channel devices by including semi-empirical correction. The impact of effective mass variation with film thicknesses is also discussed using the proposed model. All models are fully validated against the professional numerical device simulator for a wide range of device geometries.

1. Introduction

Triple gate metal oxide field effect transistors (TG MOSFET) have attracted much attention for downscaling CMOS (complementary metal oxide semiconductor) technology upto 10 nm channel length owing to its superior gate control over the channel and high current drive capability [1]. As it is difficult to dope uniformly the ultra thin body (Fin) of such transistors, undoped (or lightly-doped) body is used, and the threshold voltage is adjusted by choosing proper gate material. In such transistors, the short channel effect (SCE) is controlled by the device geometry and electrostatic integrity improves with the number of gates. The effect of quantization of electronic energies becomes significant for channel width and height below 10 nm [1] and thus it is extremely important to consider quantum effects in their threshold voltage models. Efforts have been made to include quantum effects in MOSFET models [2]. To the best of our knowledge, analytical quantum threshold voltage model for TG MOSFET has not yet been reported apart from some numerical simulation results [3,4].

In this work, we propose a physically based closed form quantum threshold voltage model for long channel TG MOSFET. The 2D Poisson equation and 2D Schrödinger equation is solved in the weak inversion region to obtain the threshold voltage model. The threshold voltage model is then extended for short channel devices using empirical correction. Impact of effective mass variation with film thicknesses are also discussed. The proposed models are then validated against data obtained from the numerical device simulator Atlas [5] for wide range of device architecture.

2. Quantum threshold voltage modeling

Fig. 1 shows the schematic diagram of an undoped body TG MOSFET. This device can be conceived as composition of a symmetric double gate (SDG) and a single gate Silicon On Insulator (SOI) transistor in perpendicular direction. In ultra thin body SDG MOSFET, quantization of electron energy is mainly due to the structural confinement. However, in single gate devices it is electronic in nature. Thus modeling of quantum threshold voltage in TG MOSFET is a tedious task. The Poisson–Schrödinger equations have to be solved consistently to obtain potential distribution and inversion charge density. But in the weak inversion regime, for undoped body, one can approximate the Poisson equation as the Laplace equation by ignoring the inversion charge density and thus decouple the two equations [6]. In the development of threshold voltage models, mid-gap metals have always been used as gate materials.

The Poisson (Laplace) equation in Silicon region for a triple gate long channel undoped body device is given by

$$\frac{\delta^2 \Phi}{\delta x^2} + \frac{\delta^2 \Phi}{\delta y^2} = 0 \tag{1}$$

* Corresponding author. Tel.: +91 80 22933090; fax: +91 80 23600808.
E-mail addresses: prakesh@cedt.iisc.ernet.in (P. Rakesh Kumar), santanu@cedt.iisc.ernet.in (S. Mahapatra).

0038-1101/$ - see front matter © 2010 Elsevier Ltd. All rights reserved.
doi:10.1016/j.sse.2010.07.013

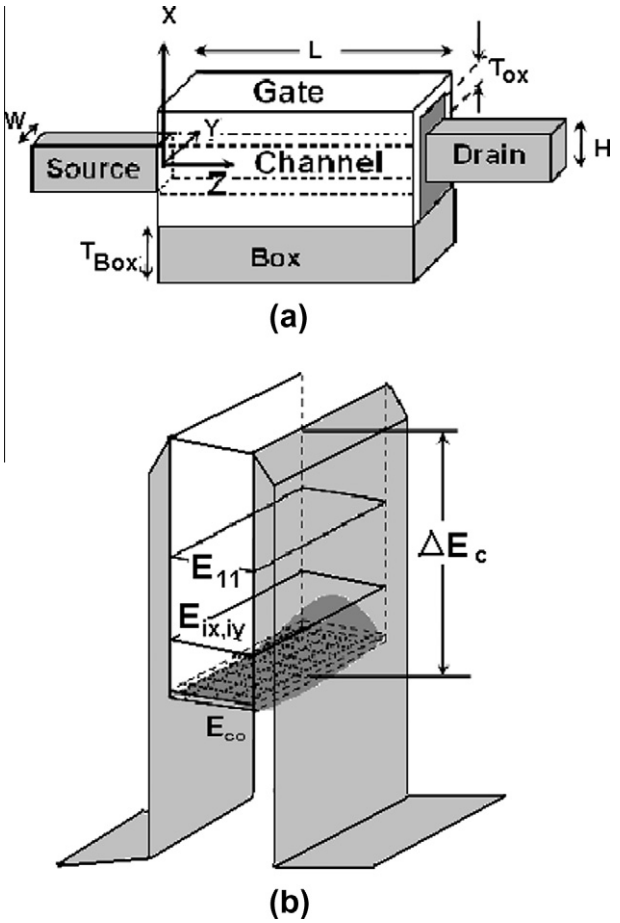

Fig. 1. (a) Schematic of triple gate transistor and (b) band diagram perpendicular to the gate in *Y* direction.

with the following boundary conditions

$$\epsilon_{si}\frac{\delta\Phi}{\delta x}\Big|_{x=\frac{H}{2}} = C_{ox}\left(V_g - \Phi\left(\frac{H}{2},y\right)\right) \tag{2}$$

$$\epsilon_{si}\frac{\delta\Phi}{\delta x}\Big|_{x=\frac{-H}{2}} = C_{box}\Phi\left(\frac{-H}{2},y\right) \tag{3}$$

$$\epsilon_{si}\frac{\delta\Phi}{\delta y}\Big|_{y=\frac{W}{2}} = C_{ox}\left(V_g - \Phi\left(x,\frac{W}{2}\right)\right) \tag{4}$$

$$\frac{\delta\Phi}{\delta y}\Big|_{y=0} = 0 \tag{5}$$

Here Φ is the electrostatic potential, V_g is the gate voltage, H and W are the height and width of the Silicon film respectively. ϵ_{si} is the permittivity of the Silicon, C_{ox} and C_{box} are the gate oxide capacitance and box capacitance respectively. T_{ox} is the gate oxide thickness and L is the channel length.

Substituting $\chi(x,y) = \Phi(x,y) - V_g$ in Eq. (1) we get

$$\frac{\delta^2\chi}{\delta x^2} + \frac{\delta^2\chi}{\delta y^2} = 0 \tag{6}$$

with the following boundary conditions

$$\epsilon_{si}\frac{\delta\chi}{\delta x}\Big|_{x=\frac{H}{2}} = -C_{ox}\left(\chi\left(\frac{H}{2},y\right)\right) \tag{7}$$

$$\epsilon_{si}\frac{\delta\chi}{\delta x}\Big|_{x=\frac{-H}{2}} = C_{box}\left(\chi\left(\frac{-H}{2},y\right) + V_g\right) \tag{8}$$

$$\epsilon_{si}\frac{\delta\chi}{\delta y}\Big|_{y=\frac{W}{2}} = -C_{ox}\left(\chi\left(x,\frac{W}{2}\right)\right) \tag{9}$$

$$\frac{\delta\chi}{\delta y}\Big|_{y=0} = 0 \tag{10}$$

Using $\chi(x,y) = G(x)\,H(y)$ we can transform Eq. (6) into

$$\frac{G''}{G} = \frac{-H''}{H} = \lambda^2 \tag{11}$$

which leads to the following general forms of solutions

$$G(x) = M\sinh(\lambda x) + N\cosh(\lambda x) \tag{12}$$

$$H(y) = P\sin(\lambda y) + Q\cos(\lambda y) \tag{13}$$

The boundary condition given in Eq. (10) forces the constant P to be zero. Hence $\chi(x,y)$ can be re-written as

$$\chi(x,y) = (A\sinh(\lambda x) + \cosh(\lambda x))B\cos(\lambda y) \tag{14}$$

where $A = M/N$ and $B = QN$ are two new constants. Using the boundary condition given in Eq. (9) in Eq. (14) we get the following eigen value expressions

$$\mu\tan\mu = \frac{W}{2}\frac{C_{ox}}{\epsilon_{si}} \tag{15}$$

where μ

$$\mu = \frac{\lambda W}{2} \tag{16}$$

The above relation gives infinitely possible values for μ and hence we obtain a series solution for $\chi(x,y)$ as

$$\chi(x,y) = \sum_n B_n\left(A_n\sinh\left(\frac{2\mu_n}{W}x\right) + \cosh\left(\frac{2\mu_n}{W}x\right)\right)\cos\left(\frac{2\mu_n}{W}y\right) \tag{17}$$

The coefficient A_n and B_n are obtained by using the boundary condition given in Eqs. (7) and (8) in Eq. (17) and could be written as

$$A_n = -\frac{\left(\frac{C_{ox}}{\epsilon_{si}} + \frac{2\mu_n}{W}\tanh\left(\frac{\mu_n}{W}H\right)\right)}{\frac{2\mu_n}{W} + \frac{C_{ox}}{\epsilon_{si}}\tanh\left(\frac{\mu_n}{W}H\right)} \tag{18}$$

$$B_n = \frac{4\sin(\mu_n)}{2\mu_n + \sin(2\mu_n)}C_n \tag{19}$$

$$C_n = \left[\frac{1}{A_nD_n - \frac{2\mu_n\epsilon_{si}}{WC_B}\sinh\left(\frac{\mu_n}{W}H\right) - \cosh\left(\frac{\mu_n}{W}H\right)}\right] \tag{20}$$

$$D_n = \frac{2\mu_n\epsilon_{si}}{HC_B}\cosh\left(\frac{\mu_n}{W}H\right) + \sinh\left(\frac{\mu_n}{W}H\right) \tag{21}$$

Finally the electrostatic potential ($\Phi = \chi + V_g$) in the Silicon region is obtained as

$$\Phi = V_g\left[\sum_n B_n\cos\left(\frac{2\mu_n}{W}y\right)\left(A_n\sinh\left(\frac{2\mu_n}{W}x\right) + \cosh\left(\frac{2\mu_n}{W}x\right)\right) + 1\right] \tag{22}$$

Fig. 2 shows a good agreement between our potential model with Atlas simulated data in the weak inversion region. It is worth noting that only first series term is used in Eq. (22) to predict the potential for thin devices accurately.

As mentioned earlier, in a TG MOSFET the energy quantization is both structural as well as electronic confinement in nature. Structural confinement arises due to the thinness of the Silicon film as electrons get confined between two Si/SiO_2 interfaces. Electronic confinement is due to the confinement of electrons in a quasi-triangular potential well formed at the interface by the conduction band of Silicon. Along the x direction confinement of electrons is mainly electronic and along the y direction, it is mostly structural in nature. It is seen from Fig. 2, the potential variation is negligible across X–Y plane. In this work we approximate the total energy quantization as purely structural in nature in both x and y directions. This approximation holds quite good for long channel devices. The energy levels can be computed by solving the following Schrödinger equation

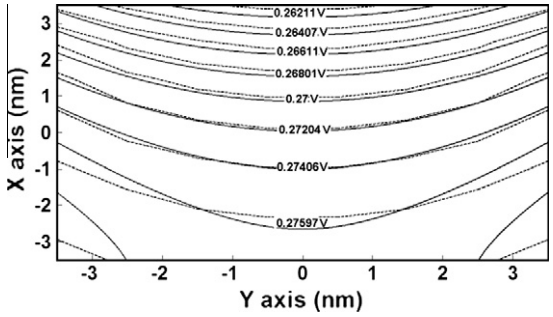

Fig. 2. 2D plot showing potential distribution in X–Y plane at $z = L/2$ at a gate voltage of 0.3 V. Here $H = 7$ nm, $W = 7$ nm, and $L = 1$ μm. Broken lines represent Atlas simulation and solid lines represent the model.

$$\frac{\hbar^2}{2m_x}\frac{\delta^2\Psi}{\delta x^2}+\frac{\hbar^2}{2m_y}\frac{\delta^2\Psi}{\delta y^2}+(E-E_{cc})\Psi=0 \tag{23}$$

where E_{cc} is given in terms of Si energy bandgap (E_g) as

$$E_{cc}=\frac{E_g}{2}-q\Phi \tag{24}$$

Potential distribution obtained in Eq. (22) is too complicated to use in Schrödinger equation in order to obtain simple analytical solution. Therefore we approximate the actual potential well as the square potential well shown by the checked lines in Fig. 1b. In the square potential well, bottom represents the minima of conduction band energy (E_{co}) at $x = H/2$ and $y = 0$ and can be given as

$$E_{co}=\frac{E_g}{2}-q\Phi(H/2,0) \tag{25}$$

Consequently the Schrödinger equation gets modified into

$$\frac{\hbar^2}{2m_x}\frac{\delta^2\Psi}{\delta x^2}+\frac{\hbar^2}{2m_y}\frac{\delta^2\Psi}{\delta y^2}+(E-E_{co})\Psi=0 \tag{26}$$

Eq. (26) can be solved by standard variable separable technique [7] and its solution Ψ and E under parabolic band approximation could be given as

$$\Psi_{i_xi_y}(x,y)=\sqrt{\left(\frac{4}{HW}\right)}\sin\left(\frac{i_x\pi\left(x-\frac{H}{2}\right)}{H}\right)\sin\left(\frac{i_y\pi\left(y-\frac{W}{2}\right)}{W}\right) \tag{27}$$

$$E_{i_xi_y}=E_{co}+\frac{\hbar^2\pi^2}{2}\left[\frac{1}{m_x}\left(\frac{i_x}{H}\right)^2+\frac{1}{m_y}\left(\frac{i_y}{W}\right)^2\right] \tag{28}$$

Here $\hbar = h/(2\pi)$, h is the Plank's constant, q is the elementary charge, Ψ is the wave function and E is the energy of the electron wave. In Silicon, there are six ellipsoidal valleys with m_t and m_l as the transverse and longitudinal effective masses, where i_x and i_y are positive natural numbers. In Eqs. (27) and (28), masses (m_x and m_y) are the effective masses along x and y directions respectively. In TG transistor energy quantization is two-dimensional in nature, i.e., along x and y direction as shown in Fig. 3. The energy valleys 1 and 2 have effective masses m_l and m_t along x and y directions. On the other hand energy valleys 3 and 4 have effective masses m_l and m_t along x and y directions and valleys 5 and 6 have effective mass m_t in the quantization directions. The energy reaches a minimum for a maximum mass as found in Eq. (28). For Silicon with six energy valleys, we have thus two lower energy valleys, two middle energy valleys and two higher energy valleys respectively. Hence the charge per unit length per valley is given by

$$Q=\sum_{i_x}\sum_{i_y}q\int_{E_{i_xi_y}}^{\infty}N_{1D}f(E)d(E) \tag{29}$$

Using N_{1D} as the one dimensional density of states and $f(E)$ as the Fermi–Dirac function Eq. (29) leads to

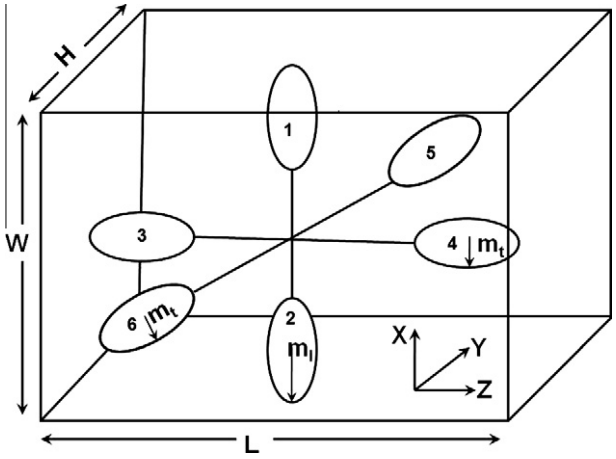

Fig. 3. Energy valleys in Silicon

$$Q=q\sum_{i_x}\sum_{i_y}\sqrt{\left(\frac{m_z}{2\pi\hbar^2}\right)}\int_{E_{i_xi_y}}^{\infty}\frac{(E-E_{i_xi_y})^{\frac{-1}{2}}}{1+\exp\left(\frac{E-E_F}{kT}\right)}dE \tag{30}$$

Here m_z is the mass of the valley perpendicular to the direction of quantization. The charge Eq. (30) is difficult to solve. However in the weak inversion regime, the Fermi level is found to be much below the conduction band energy. Hence, using Boltzmann statistics the integrated charge could be approximated as

$$\begin{aligned}Q&=q\sqrt{\left(\frac{m_z}{2\pi\hbar^2}\right)}\sum_{i_x}\sum_{i_y}\int_{E_{i_xi_y}}^{\infty}\frac{\exp\left(\frac{E_F-E}{kT}\right)}{\sqrt{(E-E_{i_xi_y})}}dE\\&=q\sum_{i_x}\sum_{i_y}\sqrt{\frac{m_zkT}{2\hbar^2}}\exp\left(\frac{E_F-E_{i_xi_y}}{kT}\right)\end{aligned} \tag{31}$$

Using Eqs. (28) and (31), the total integrated charge could be rewritten as

$$\begin{aligned}Q=&\sum_{i_x}\sum_{i_y}q\\&\times\sqrt{\frac{2kTm_t}{\hbar^2}}\left(\exp\left(-\frac{E_{co}+\kappa(i_x,i_y)}{kT}\right)+\exp\left(-\frac{E_{co}+\varpi(i_x,i_y)}{kT}\right)\right)\\&+\sum_{i_x}\sum_{i_y}q\sqrt{\frac{2kTm_l}{\hbar^2}}\exp\left(-\frac{E_{co}+\omega(i_x,i_y)}{kT}\right)\end{aligned} \tag{32}$$

where

$$\kappa(i_x,i_y)=\frac{\hbar^2\pi^2}{2}\left[\frac{1}{m_l}\left(\frac{i_x}{H}\right)^2+\frac{1}{m_t}\left(\frac{i_y}{W}\right)^2\right] \tag{33}$$

$$\varpi(i_x,i_y)=\frac{\hbar^2\pi^2}{2}\left[\frac{1}{m_t}\left(\frac{i_x}{H}\right)^2+\frac{1}{m_l}\left(\frac{i_y}{W}\right)^2\right] \tag{34}$$

$$\omega(i_x,i_y)=\frac{\hbar^2\pi^2}{2}\left[\frac{1}{m_t}\left(\frac{i_x}{H}\right)^2+\frac{1}{m_t}\left(\frac{i_y}{W}\right)^2\right] \tag{35}$$

Fig. 4 shows the population of electrons in each subband and the distribution of subbands in the channel region. The first subscript in the energy denotes the valley (1–3 for lower, middle and higher valleys respectively) and the second subscript denotes the energy level in that valley. Thus solid, horizontal and vertical lines indicate the lower, middle and higher valleys respectively. It is observed that the charge decays with increase in energy levels in each valley. It is also seen from Fig. 4 that only one energy level

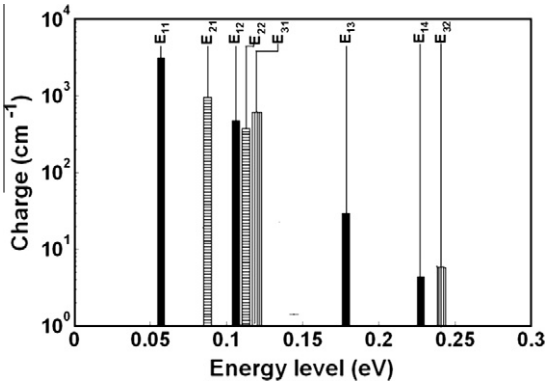

Fig. 4. Population of electron concentration in each subband at V_g of 0.3 V for a long channel device having W = 5 nm and H = 7 nm. Solid, horizontal and vertical lines indicates the lower, middle and higher valley respectively.

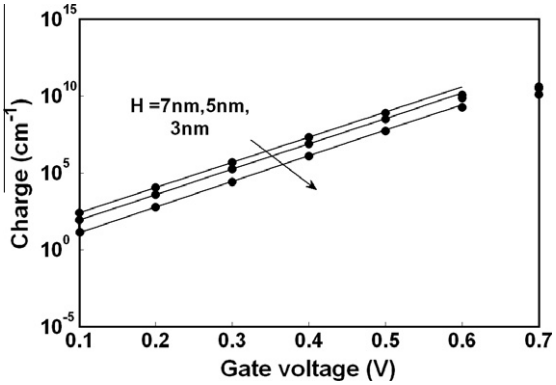

Fig. 6. Plot of integrated charge with gate voltage for different film heights at width = 5 nm. Symbols represent Atlas simulation and lines represent the model.

each in lower, middle and higher energy valleys is sufficient to predict the charge accurately. Hence only one energy level is used in the further analysis.

Threshold voltage for undoped body devices is defined [8,9] as the gate voltage when the integrated charge becomes equal to the critical threshold charge ($Q_T = 5 \times 10^{24}$ qWH cm^{-1}). Using Eq. (32) the threshold voltage is obtained as

$$V_T = \frac{\frac{E_g}{2q} + \frac{kT}{q}\ln\left(\frac{Q_T}{\rho}\right)}{B_1\left(A_1\sinh\left(\frac{H\mu_1}{W}\right) + \cosh\left(\frac{H\mu_1}{W}\right)\right) + 1} \tag{36}$$

where ρ is given by

$$\rho = q\sqrt{\frac{2kTm_t}{\hbar^2}}\left(\exp\left(-\frac{\kappa(1,1)}{kT}\right) + \exp\left(-\frac{\varpi(1,1)}{kT}\right)\right) + q \times \sqrt{\frac{2kTm_l}{\hbar^2}}\exp\left(-\frac{\omega(1,1)}{kT}\right) \tag{37}$$

3. Results and discussion

Fig. 5 shows the charge distribution plot at gate voltage of 0.5 V. The charge distribution along y-axis is plotted for various x values. The keyword 2DXY.SCHRO is used in Atlas to involve the two-dimensional Poisson–Schrodinger Solver. The keywords NUM.DIRECT along with SP.DIR are used to select the valleys with appropriate effective mass [5]. Fig. 6 represents the plot of total integrated charge with the gate voltage. It is seen from the figure that threshold voltage increases with the decrease in film thickness because of energy quantization.

Eq. (32) is used to obtain the integrated charge with only one energy level and one series term. Fig. 7 shows the plot of probability density function (Ψ^2) of electrons for first two energy levels.

In literature there is no standard value for the threshold charge (Q_T). Some authors [10] have equated the threshold charge to thermal charge. However, we have found by numerical simulation that the threshold voltage obtained by using the thermal charge sometimes (depending on device geometry) lies in the strong inversion regime and thus over predicts the threshold voltage. In this work we first extract the threshold voltage from classical simulation of $I_d - V_g$ characteristics by linear interpolation method for wide range of device architectures. Corresponding to the extracted threshold voltage, integrated charge at virtual cathode is computed for each device and the average charge is taken as the threshold charge which is 5×10^{24} qWH cm^{-1}. Note that for using the proposed model for compact modeling purpose, one does not need to repeat the above mentioned numerical simulation exercise. Same value of the threshold charge is applicable to all practical device geometries for obtaining accurate value of the threshold voltage.

In Fig. 8 black and grey colours show the variation of threshold voltage with film height and width respectively. When the film width is lesser than the film height, the device behaves more like a symmetric double gate MOSFET. On the other hand, when the film height is lesser than the film width, the device behaves like a single gate SOI MOSFET. As for the same dimensions the threshold voltage of symmetric double gate MOSFET gives lower thresh-

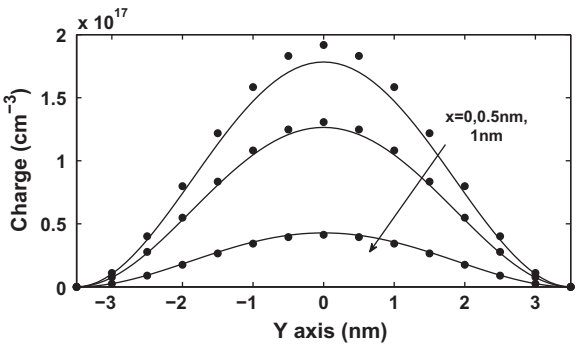

Fig. 5. Charge distribution plot for long channel TG MOSFET along y-axis for different x values at V_g = 0.5 V having H = 3 nm, and W = 7 nm. Symbols represent Atlas simulation and lines represent the model.

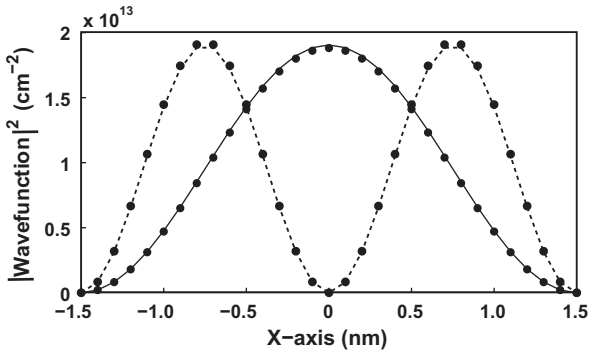

Fig. 7. The plot of probability density function in x direction. Solid and dotted line correspond to first and second energy levels respectively and calculated by the proposed model. Symbols corresponds to the Atlas simulation. Here W = 3 nm and H = 7 nm.

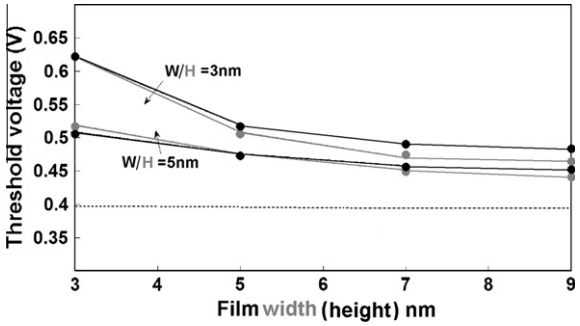

Fig. 8. Variation of long channel quantum threshold voltage with film height/film width. Symbols and lines represent the Atlas quantum simulation and the model respectively. Black and grey colour indicates the plot when width is held constant with varying height and height is held constant with varying width respectively. Dotted line shows the variation of classical threshold voltage with film height at $W = 3$ nm.

old voltage compared to SOI transistor, the black line goes above the grey line after attaining equal film height and width. Dotted line shows the variation of classical threshold voltage with film height at $W = 3$ nm. It is seen from the figure that the difference between classical and quantum threshold voltage increases with decrease in the film height due to the quantum effects.

Physical modeling of threshold voltage for a short channel TG device is a difficult task mainly due to (i) difficulty in obtaining the analytical solution of the 3D Poisson (Laplace) equation and (ii) the confinement cannot be assumed to be fully structural in nature. In this work we have, however, been able to extend the long channel model to short channel devices (for low drain voltage) by the empirical relationship:

$$V_T(L) = V_T - 1.6V_{bi}\left(\frac{WH}{L^2}\right)^m \tag{38}$$

where V_{bi} is the build in potential in a $p^+ - i$ diode. Here m is the fitting parameter which depends only on the film width and takes the values 2, 1.95, 1.75, and 1.5 for film widths $W = 9$ nm, 7 nm, 5 nm, and 3 nm respectively. Fig. 9 shows the variation in threshold voltages with width and height of the film at channel length of 20 nm at low drain voltages. Eq. (38) is used to obtain the threshold voltage plot in Fig. 9. Fig 10 shows the plot with variation in threshold voltage with film widths at film height of 9 nm for different channel lengths. Vertical spacing gives the short channel effect. It is observed that the short channel effects are quite accurately captured by the empirical relationship.

So far in the discussion, we assumed the value of the effective masses to be equal to the value of bulk Silicon effective masses.

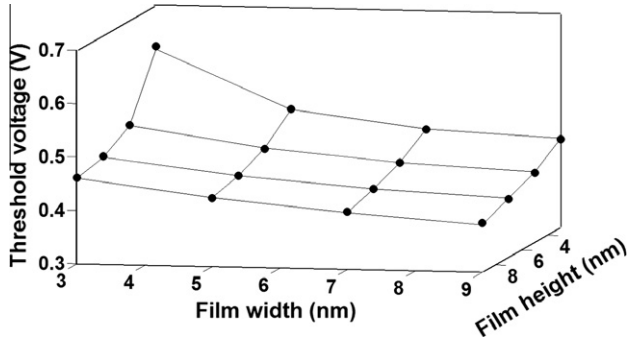

Fig. 9. Variation of quantum threshold voltage with film height and width for channel length $L = 20$ nm. Symbols and lines represent the Atlas simulation and model respectively.

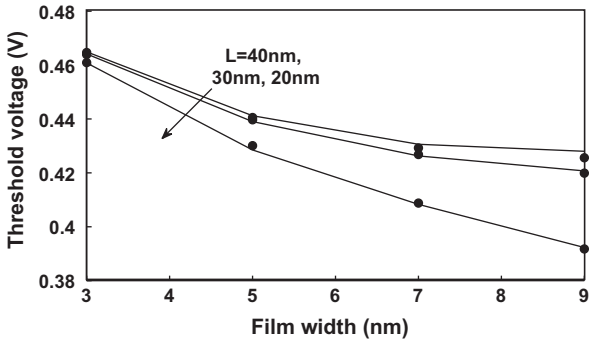

Fig. 10. Variation of quantum threshold voltage with film width for various channel lengths at $H = 9$ nm. Symbols and lines represent the Atlas quantum simulation and model respectively.

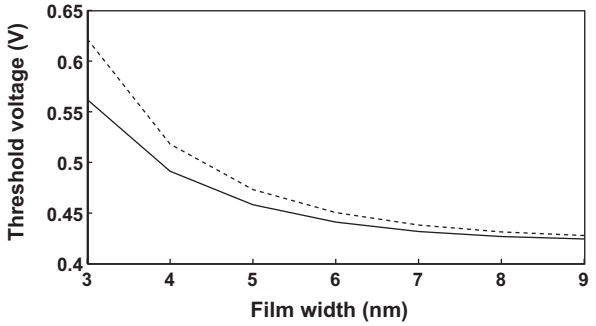

Fig. 11. Variation of long channel quantum threshold voltage with film width at different effective mass at $H = W$. Solid and dotted line shows the variation of quantum threshold voltage if bulk and effective mass obtained by Eq. (39) is used in threshold voltage model.

However the values of effective masses change with film thickness. For a cylindrical body Silicon nanowire transistor, having a diameter d, the change in effective mass could be formulated as a function of d by following [11] Eq. (39)

$$m^*_{l,t}(d) = m^*_{l,t}(\infty)\left(1 + \frac{a_{l,t}}{d} + \frac{b_{l,t}}{d^2}\right) \tag{39}$$

where $a_{l,t}$ and $b_{l,t}$ are the fitting parameters having the values $a_l = 0$, $a_t = 0.68$, $b_l = 0.28$, and $b_t = 0.87$. $m^*_{l,t}(\infty)$ denotes the effective mass in bulk Silicon. In this work we approximated the value of equivalent nanowire diameter to be equal to $(W + H)/2$. In Fig. 11 dotted line shows the variation of threshold voltage if we use the constant bulk effective mass and black line shows the variation of threshold voltage if we use effective mass obtained using Eq. (39). The figure shows that the threshold voltage is low when we consider effective mass dependence on device geometry rather than assuming it to be a constant.

4. Conclusions

A physically based analytical quantum threshold voltage model for a long channel triple gate MOSFET is developed and verified against professional numerical simulator. The proposed model, based on the solutions of Poisson and Schrödinger equations, is capable of predicting the threshold voltage for ultra thin body devices. Model is extended for short channel devices using empirical correction. The impact of effective mass variation with channel thickness is also discussed.

Acknowledgment

This work is funded by Department of science and Technology (DST), India under Grant SR/S3/EECE/047/2008.

References

[1] Colinge JP. FinFETs and other multi-gate transistors. Springer; 2007.
[2] Lallement Christophe, Sallese Jean-Michael, Bucher Matthias, Grabinski Wladek, Fazan Pierre C. Accounting for quantum effects and polysilicon depletion from weak to strong inversion in a charge-based design-oriented MOSFET model. IEEE Trans Electron Dev 2003;50(2):406–17.
[3] Colinge et al. Quantum Mechanical effects in trigate SOI MOSFETs. IEEE Trans Electron Dev 2006;53(5):1131–6.
[4] Yan R, Afzalian A, Lee C-W, Dehdashti Akhavan N, Xiong W, Colinge J-P. Quantum3D simulation and measurement of very narrow AM and IM triple-gate MOSFETs. In: Proceedings of China–Ireland international conference on information and communication technologies (CIICT 2008), September 2008, p. 627–30.
[5] Atlas user manual,version 5.14.0.R. <www.silvaco.com>.
[6] Trivedi Vishal P, Fossum Jerry G. Quantum-mechanical effects on the threshold voltage of undoped double-gate MOSFETs. IEEE Electron Dev Lett 2005;26(8):579–82.
[7] Kreyszig Erwin. Advanced engineering mathematics. John Wiley and sons; 2005.
[8] Andreas et al. Threshold voltage model for short-channel undoped symmetrical double-gate MOSFETs. IEEE Trans Electron Dev 2008;55(9):2512–6.
[9] Hamid et al. Analytical model of the threshold voltage and subthreshold swing of undoped cylindrical gate-all-around-based MOSFETs. IEEE Trans Electron Dev 2007;54(3):572–9.
[10] Munteanu et al. Quantum short channel compact model for the threshold voltage in double gate MOSFETs with high-permittivity gate dielectrics. J Non-cryst Solids 2005;351:1911–8.
[11] Gnani E, Reggiani S, Rudan M, Baccarani G. Effects of the band-structure modification in silicon nanowires with small diameters. In: Solid state device research conference, 2006, p. 170–3.